Application of a Semiempirical Analytical Model to Predict Erosion of a Texas Coastal Defense Dune System during Storms under Climate Change

Seokmin Son, S.M.ASCE[1]; Meri Davlasheridze, Ph.D.[2]; Ashley D. Ross, Ph.D.[3]; and Jeremy D. Bricker, Ph.D., P.E., M.ASCE[4]

Abstract: This study assesses the feasibility of a beach and dune system as flood defense against storm surge along the coastlines of the Houston–Galveston area, proposed as a part of the Coastal Texas Project. We apply a semiempirical analytical model to predict dune erosion in a dual-dune system under changing climate conditions. Synthetic storms were simulated using validated hydrodynamic, wave, and hurricane models to produce input data (storm surge, wave height, and period) for the dune erosion model, reflecting both present day and future climate scenarios that incorporate projected sea level rise (SLR). Bias-correction techniques were applied to climate model output using historical observations of storm surge and wave data. An alternative sampling approach was also developed to stochastically predict dune erosion by integrating synthetic data into a copula-based framework. Results indicate that the annual-average dune erosion is approximately 8%–10% of system volume in the present scenario and increases to 33%–40% in future scenarios with higher SLR, leading to estimated dune rehabilitation cycles of 8–10 and 2–2.5 years, respectively. These findings suggest that, although the proposed beach and dune system is likely to be effective for storm surge protection under the present climate condition, significant adjustments will be desirable to maintain its resilience in the face of evolving climate and sea level rise. Importantly, bias correction of input data yielded substantial reductions in predicted storm surge and significant wave height, resulting in more accurate dune erosion predictions. This demonstrates the necessity of bias correction of hydrodynamic and wave parameters derived from global climate simulations for reliable coastal risk assessment and future planning. The copula sampling approach produced results comparable to the original results, which considered storms with extremely low or high occurrence probabilities, while providing lower sensitivity to bias-correction methods and copula generator types.
DOI: 10.1061/JWPED5.WWENG-2447

Author keywords: Beach and dune system; Flood defense; Dune erosion model; Synthetic storm; Sea level rise; Bias correction; Annual-average dune erosion; Copula sampling approach.

Introduction

In coastal communities, dunes serve as primary flood defense lines against coastal flooding from high storm surges and waves during severe storms (Cooper 1958; Larson et al. 2004; Li et al. 2014; Mull and Ruggiero 2014; Ciavola et al. 2015). As such, dunes are directly exposed to these natural hazards, which are likely to cause dune erosion through collision or overwash, thereby reducing dune reliability (Sallenger 2000). If dunes are breached or overtopped by extreme waves, the communities behind them are likely to experience severe flooding and extensive damage (Larson et al. 2004; Figlus et al. 2011; Mull and Ruggiero 2014). Poststorm dune nourishment is essential to adequately protect people and property, although the process entails significant costs. In addition, dune erosion is projected to worsen due to future climate change. More frequent intense storms are expected to occur along coastlines (Knutson and Tuleya 2004; Emanuel 2005; Webster et al. 2005), and rising sea levels will further increase vulnerability of coastal dunes to erosion (Bruun 1962; Carter 1991; Davidson-Arnott 2005; Feagin et al. 2005). This study examines a place where these processes are unfolding rapidly—Galveston Island, Texas, is highly vulnerable to hurricanes and is experiencing a higher rate of sea level rise (SLR) than the global average (Gray 2024).

After Hurricane Ike struck the Houston–Galveston Area (HGA) and caused serious damage in 2008, the Ike Dike emerged as a flood defense concept to protect the region against future storm surges (Merrell et al. 2011). Now fully developed and integrated into the USACE Coastal Texas Project, the storm surge barriers are part of a multifaceted defense system that includes a sandy beach and dune component along the coastlines of the West Galveston Island and the Bolivar Peninsula, as shown in Fig. 1 (USACE Galveston District and GLO 2021a). The sandy system features a dual-dune system with a 4.27-m (NAVD88) landward

[1]Ph.D. Candidate, Dept. of Civil and Environmental Engineering, Univ. of Michigan, Ann Arbor, MI 48109. ORCID: https://orcid.org/0009-0009-7207-351X. Email: seokmins@umich.edu

[2]Associate Professor, Dept. of Marine and Coastal Environmental Science, Texas A&M Univ., Galveston, TX 77553. Email: davlashm@tamug.edu

[3]Associate Professor, Dept. of Marine and Coastal Environmental Science, Texas A&M Univ., Galveston, TX 77553. Email: ashleydross@tamug.edu

[4]Associate Professor, Dept. of Civil and Environmental Engineering, Univ. of Michigan, Ann Arbor, MI 48109; Associate Professor, Faculty of Civil Engineering and Geosciences, Delft Univ. of Technology, 2628 CN Delft, Netherlands (corresponding author). ORCID: https://orcid.org/0000-0002-7503-6652. Email: jeremydb@umich.edu

Note. This manuscript was submitted on October 23, 2025; approved on February 18, 2026; published online on April 10, 2026. Discussion period open until September 10, 2026; separate discussions must be submitted for individual papers. This paper is part of the ***Journal of Waterway, Port, Coastal, and Ocean Engineering***, ASCE, ISSN 0733-950X.

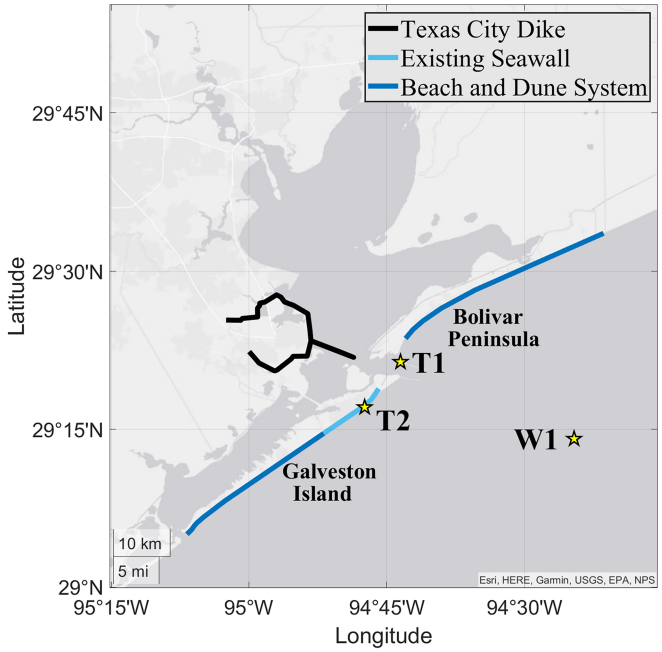

Fig. 1. HGA with profiles of the proposed beach and dune system. (Map source: Esri, HERE, Garmin, USGS, EPA, NPS.)

dune and a 3.66-m (NAVD88) seaward dune, which are improved from the existing dune profile. This type of barrier is projected to enhance the natural resiliency of the system and to maintain it over time, aiming to minimize environmental and social impacts while significantly reducing coastal flood risk.

However, concerns were raised about the effectiveness of the USACE beach and dune system in mitigating storm surge risk, with suggestions that the system may need to be strengthened beyond what is currently planned (Merrell et al. 2021). Compared to earlier proposals for the coastal spine by Jonkman et al. (2015) or Ebersole et al. (2018), which featured a 5.18-m (NAVD88) barrier system, the USACE design may not be sufficiently tall to protect the HGA from severe storms (Merrell et al. 2021), which are expected to become more frequent in the future (Knutson and Tuleya 2004). In addition, concerns have been raised that the proposed dune components may not be able to withstand storm surges between beach nourishment cycles, which are expected to occur every 5–8 years. This could leave the region vulnerable to coastal flooding. As an alternative, a more robust barrier system was recommended, utilizing core-enhanced dunes or hybrid coastal structures instead of natural dunes (Merrell et al. 2021). This approach would help maintain dune heights during severe storms and reduce the sand volume required for nourishment, which is increasing in cost and supply (Parkinson and Ogurcak 2018; de Schipper et al. 2021), while also preserving the system's natural resiliency. To determine whether the natural beach and dune system remains effective as a flood defense, it is imperative to evaluate dune erosion during severe storms under both present and future climate conditions.

In this study, we evaluated the expected erosion of the Coastal Texas Project dune system, considering synthetic storm events, both under present and future climate conditions and with different SLR projections. A semiempirical analytical model developed by Larson et al. (2004) was used to calculate dune erosion rates as a function of storm surge levels, significant wave heights, and mean absolute wave periods. These hydrodynamic and wave parameters were produced through storm surge simulations using Delft3D Flexible Mesh (D-Flow FM) coupled with Simulating Waves Nearshore (SWAN), and the empirical transport coefficient of the model was calibrated using USACE's estimates of dune erosion during historical storms (USACE Galveston District and GLO 2021c). To align with historical climate data, a bias-correction technique was applied to the modeled storm surge and wave data using historical observation data for reference, and these bias-corrected (BC) data served as input variables for the dune erosion model. Finally, the total dune erosion volumes were estimated for all synthetic storms and used to predict probabilistic and annual-average dune erosion volumes, accounting for evolving storm frequency.

Additionally, we also developed a new stochastic method to provide an alternative prediction for dune erosion: a copula sampling approach. Dune erosion has long been recognized as a critical issue in coastal engineering. Numerous analytical models have been developed to predict dune erosion under various storm conditions (Kriebel and Dean 1993; Larson et al. 2004; van Rijn 2009). The joint probability method (JPM) has been used to estimate extreme storm event probabilities to analyze dune erosion with multiple wave parameters (Callaghan et al. 2008; Ranasinghe et al. 2012), and the copula approach has been incorporated into the JPM (Corbella and Stretch 2012; Li et al. 2014; Enríquez et al. 2019). In this study, our approach incorporates synthetic storm data into an Archimedean copula framework based on Larson et al. (2004) to predict future storm-induced dune erosion considering both intensifying storm climatology and SLR projections. Probability distributions of the bias-corrected data were used to sample each variable while preserving their correlations, enabling probabilistic prediction of dune erosion as well. The results from the copula sampling approach were compared to those obtained from direct synthetic storm simulations to evaluate the method's accuracy and robustness. From this study, we obtained information on the effectiveness of the beach and dune system as a future flood defense strategy under evolving climate conditions. Furthermore, the new approach we developed extended previous analytical and probabilistic methods by integrating bias-corrected storm data with copula-based sampling, offering advanced stochastic estimates of future dune erosion in response to changing climate conditions.

Data and Methods

Dune Erosion Model

Sallenger (2000) suggested a four-level storm impact scale for dune and beach systems: (1) swash regime, (2) collision regime, (3) overwash regime, and (4) inundation regime. In the swash regime, sediment is transported offshore but replaced, resulting in minimal net change. In the collision regime, sediment is transported offshore and not returned, leading to net erosion. In the overwash and inundation regimes, sediment is transported landward, causing the dune to migrate in that direction. Assuming there is zero net erosion in the swash regime and regarding the inundation regime as equivalent to the overwash regime (since the still water level was not expected to exceed the dune crest of the proposed system), we focused only on the collision and overwash regimes when modeling dune. A semiempirical analytical model developed by Larson et al. (2004) assessed dune erosion during extreme storm events in the collision regime, while Larson et al. (2009) extended the model to account for reduced impact force in the overwash regime. Both models are based on wave impact

theory as follows:

$$q_D = \begin{cases} 4C_s \dfrac{(R_{up} + \mathrm{SWL} - z_d)^2}{T} & \text{collision regime} \\ 4C_s \dfrac{(R_{up} + \mathrm{SWL} - z_d)(Z_d - z_d)}{T} & \text{overwash regime} \end{cases} \quad (1)$$

where q_D = dune erosion rate along a section (m^2/s); C_s = empirical transport coefficient; R_{up} = wave runup; z_d = dune toe level; Z_d = dune crest level; SWL = still water level, which is the combination of astronomical tide and storm surge (S); and T = swash period, which is equivalent to a mean absolute wave period or a spectral mean wave period (T_m). The wave runup in this model is empirically calculated as follows (Larson et al. 2004; Holthuijsen 2007):

$$R_{up} = 0.158\sqrt{H_o L_o}, \quad H_o = \frac{H_{s,o}}{\sqrt{2}}, \quad L_o = \frac{gT_m^2}{2\pi} \quad (2)$$

where H_o = wave height; L_o = mean wavelength; and $H_{s,o}$ = significant wave height, all in deep water. H_o is taken as the root-mean-square wave height under the assumption of a Rayleigh distribution (Larson et al. 2016).

Since the wave data are not always retrieved from deep water, the significant wave height and wavelength values were adjusted by wave de-shoaling as follows (Sorensen 2006):

$$H_{s,o} = \frac{H_s}{K_s K_r} \quad (3)$$

where H_s = retrieved significant wave height; K_s = shoaling coefficient; and K_r = refraction coefficient, assumed to be 1 in this study. K_s is calculated from wave-energy flux conservation as the ratio of group velocity as follows:

$$K_s = \sqrt{\frac{C_{g,o}}{C_g}}, \quad C_{g,o} = \frac{gT_m}{4\pi}, \quad C_g = \frac{1}{2}\left(1 + \frac{2\mathrm{kh}}{\sinh(2\mathrm{kh})}\right)\frac{L_m}{T_m} \quad (4)$$

where $C_{g,o}$ = group velocity in deep water; and C_g, h, k, and L_m = group velocity, water depth, wavenumber, and mean wavelength at the location of data retrieval, respectively. L_m was computed using the wave dispersion relation by the iterative method with a tolerance of 1×10^{-5}

$$\omega^2 = \left(\frac{2\pi}{T_m}\right)^2 = g\left(\frac{2\pi}{L_m}\right)\tanh\left(\frac{2\pi h}{L_m}\right) \quad (5)$$

where ω = wave angular frequency.

In the overwash regime, some of the eroded sediment is transported landward as overwash (q_L), while the rest is moved seaward as backwash (q_S), with the ratio between these two rates given by $\alpha = q_L/q_S$. Sand transport rates are then calculated as follows:

$$q_L = \frac{\alpha}{1+\alpha} q_D, \quad q_S = \frac{1}{1+\alpha} q_D, \quad \alpha = \frac{1}{C_e}\left(\frac{R_{up} + \mathrm{SWL} - z_d}{Z_d - z_d} - 1\right) \quad (6)$$

where C_e = empirical coefficient, set to 3 (Larson et al. 2009). The schematic concepts of dune erosion in the collision and overwash regimes are illustrated in Fig. 2.

However, because the analytical models are one-dimensional in the horizontal direction, they cannot account for variations in wave direction. To address this, recognizing that wave incidence angle influences dune erosion (Kobayashi et al. 2009) and that the force component is explicitly represented as a cosine function (Dean and Dalrymple 1991), we simply incorporated the mean wave direction into our analysis by multiplying cos ϕ by Eq. (1), where ϕ is the wave incidence angle ($\phi = 0°$ for waves normal to the dune). If $\phi > 90°$ (waves propagating away from the shore), the erosion rate is set to zero. This erosion rate was computed at every time step and then integrated over the storm duration to estimate the total volume of dune erosion. It is important to note that this bulk analysis considers only cross-shore processes to quantify storm-driven dune erosion associated with offshore sediment losses. Longshore sediment transport, which primarily redistributes sediment along the coastline rather than removing sediment from the beach and dune system, is therefore not explicitly considered.

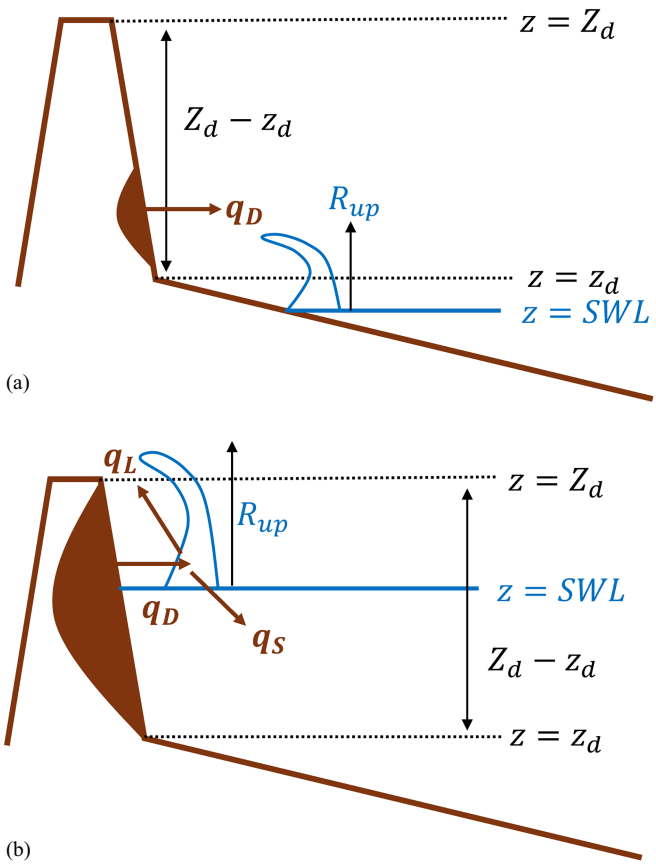

Fig. 2. Schematic concepts of dune erosion: (a) collision regime; and (b) overwash regime.

We applied these models to the Coastal Texas Project dune system, which features a dual-dune design. The seaward dune has a crest elevation of 3.66 m (NAVD88) and a toe elevation of 1.22 m (NAVD88), while the landward dune has a crest elevation of 4.27 m (NAVD88) and a toe elevation of 1.83 m (NAVD88). The profile areas for the seaward and landward dunes are approximately 35.37 and 43.54 m^2, respectively. The dunes on West Galveston and Bolivar Peninsula beaches span about 29 and 40 km, respectively. For modeling simplicity, the landward dune was assumed to begin eroding only after the seaward dune was fully eroded. Although this may not strictly reflect the physical sequence of storm events, it provides a practical way to partition erosion while preserving the cumulative sediment loss. Given that the primary interest of the study is to estimate the overall volume of dune erosion rather than to resolve the temporal evolution of dune morphology during storms, this assumption is expected to have only a limited influence on the results of predicted dune erosion.

Synthetic Storm Simulations

In this study, synthetic storm tracks were used to predict storm-induced dune erosion to account for storm conditions under both present and future climates. The synthetic storms were statistically downscaled from a CMIP6 general circulation model (GCM), the Hadley Centre Global Environmental Model (HadGEM), provided by WindRiskTech, New Harbor, ME (Emanuel et al. 2008). Each track provides center latitude and longitude, central surface pressure, maximum 10-m wind speed, and the radius of maximum winds at 2-h intervals. Two storm data sets were used: one representing present-day climate based on simulations under 20th century conditions, and the other representing future climate following the Intergovernmental Panel on Climate Change (IPCC) SSP5-8.5 pathway (IPCC 2023). Each data set consists of 150 storm tracks per year, totaling 4,500 tracks over the 30 years (present: 1981–2010; future: 2071–2100). However, we focused only on storms likely to significantly affect the HGA, filtering the synthetic storms by landfall location and storm intensity (Son et al. 2025). This selection is intended to target physically meaningful data while maintaining feasible computational costs. As a result, 115 storm tracks were selected and simulated for the present climate, and 158 for future climate conditions.

Synthetic storm simulations were conducted in D-Flow FM coupled with SWAN, using a two-way wave–current interaction (Deltares 2024a, b), across the northwest Gulf of Mexico with increased resolution over the HGA. To represent spatially varying land roughness, Manning's n coefficients were assigned to each grid cell based on land cover classification (Bunya et al. 2010), while a constant value of $n = 0.015$ was specified over the ocean. The maximum Courant number was set at 0.5, and model outputs were recorded at 1-h intervals. More details on D-Flow FM data sources are presented in Table 1. The synthetic storms served as meteorological boundary conditions of the model after being converted into pressure and wind velocity fields using the Holland (1980) model. Model parameters were estimated following Holland et al. (2010), and storm asymmetry was represented by incorporating a wind vector approach based on Xie et al. (2006) and Kalourazi et al. (2020), with inflow angles as described by Graham and Nunn (1959). The accuracy of hydrodynamic, wave, and hurricane models was validated by comparing their outputs against observations throughout the Galveston Bay during Hurricane Ike (2008), with overland inundation extent and depth estimates from the Harris County Flood Control District (for details, see Son et al. 2025).

For future storm simulations, relative SLR was incorporated into the initial water level conditions as the sum of global and regional components. Global SLR projections, mainly caused by global warming and depending heavily on greenhouse gas emission scenarios, were based on the SSP5-8.5 pathway to be consistent with the GCM scenario. Assuming a steady global SLR for future storm events, it was estimated for the year 2085 relative to the baseline of 2000. To address uncertainty, three global SLR scenarios were considered: 0.48, 0.57, and 0.75 m (IPCC 2023). Regional SLR, accounting for factors such as changes in ocean circulation and vertical land motion, was estimated at 0.51 m by 2085 relative to 2000 (Sweet et al. 2022). Combining these components, three relative SLR scenarios were established for the study: 0.99 m (low SLR), 1.08 m (middle SLR), and 1.26 m (high SLR). These SLR scenarios were added to the mean higher high water (MHHW) level of 0.18 m, which was assumed to be constant across all locations in the integrated model (Ke et al. 2021).

Bias Correction

While GCMs are valuable tools for understanding and predicting present and future climate changes, they often contain systematic errors due to their limited resolution, which can hinder the accurate capture of regional features (Grotch and Maccracken 1991; Fowler et al. 2007; Maraun 2016). Therefore, it is desirable to apply bias-correction techniques to improve model accuracy and ensure that the model output is statistically consistent with observed data, particularly for extreme events (Hagemann et al. 2011; Teutschbein and Seibert 2012; Maraun 2016). Bias correction has been commonly used for climate variables such as precipitation or temperature (Hagemann et al. 2011; Teutschbein and Seibert 2012; Cannon et al. 2015; Um et al. 2016), as well as for model outputs including storm surges (Lin et al. 2016; Cid et al. 2018) and significant wave heights (Lemos et al. 2020; Lobeto et al. 2021; Loarca et al. 2023). When applying bias correction to temporally evolving storm-driven data, correcting the entire time series (TS) is ideal for preserving the dependence structure among variables. However, since individual storms have different durations that result in varying numbers of time steps, a consistent bias correction of time series across all storms is practically challenging. Therefore, in this study, bias correction was instead applied to the extreme values of D-Flow FM and SWAN output variables (S, H_s, and T_m) obtained from each synthetic storm. Throughout this study, S is presented in meters relative to MHHW to isolate the storm-induced surge height from the mean sea level (including SLR) and astronomical tides.

This study employed the quantile mapping (QM) technique to correct errors in the present-day data set (1981–2010), which aligns the cumulative distribution functions (CDFs), representing nonexceedance probabilities, of modeled and observed data as follows (Cannon et al. 2015):

$$\hat{x}_{m,p} = F_{o,h}^{-1}\{F_{m,h}(x_{m,p})\} \tag{7}$$

where $x_{m,p}$ = modeled data in the projected period (non-bias-corrected, non-BC); $F_{m,h}$ = CDF of the modeled data within a historical period; $F_{o,h}$ = CDF of the observed data; and $\hat{x}_{m,p}$ = bias-corrected data of $x_{m,p}$. The subscriptions m represents modeled, o observed, p the projected period, and h the historical period. This technique is valid only when the projected period falls within the range of the historical period, as it assumes that the observed data remains stationary. However, when applying bias correction to future modeled data, it becomes challenging to account for future climate changes. Alternatively, for the future data set

Table 1. Data sources for D-Flow FM configuration

Data type	Source	Reference
Global bathymetry	General Bathymetric Chart of the Oceans (GEBCO)	GEBCO Compilation Group (2023)
High-resolution topography	National Oceanic and Atmospheric Administration (NOAA) National Centers for Environmental Information (NCEI) Coastal Relief Model	NOAA and NCEI (2023)
Land cover classification	National Land Cover Database (NLCD)	Dewitz (2023)
Air-sea drag coefficient	A Sea Drag Relation for Hurricane Wind Speeds	Zweers et al. (2010)

(2071–2100), the quantile delta mapping (QDM) technique was used, which preserves relative changes in quantiles and thus accounts for differences between historical and future climates (Cannon et al. 2015)

$$\hat{x}_{m,p} = \hat{x}_{o;m,,h;p}\Delta_m$$
$$\hat{x}_{o;m,,h;p} = F_{o,h}^{-1}\{F_{m,p}(x_{m,p})\},$$
$$\Delta_m = \frac{F_{m,p}^{-1}\{F_{m,p}(x_{m,p})\}}{F_{m,h}^{-1}\{F_{m,p}(x_{m,p})\}} = \frac{x_{m,p}}{F_{m,h}^{-1}\{F_{m,p}(x_{m,p})\}} \quad (8)$$

where $\hat{x}_{o;m,,h;p}$ = bias-corrected data of $x_{m,p}$ before considering relative changes; Δ_m = relative change in quantiles between the historical period and the projected period; and $F_{m,p}$ = CDF of the modeled data in the projected period.

Both nonparametric and parametric methods were used to construct CDFs, for comparison of results and evaluation of bias-correction uncertainty. For the nonparametric approach, empirical CDFs estimated the nonexceedance probabilities of extreme data, with linear interpolation applied for smooth mapping. The parametric method involved fitting all observed and modeled data of S, H_s, and T_m to the generalized extreme value (GEV) distribution using maximum likelihood estimation. For more details on probability distributions and goodness of fit, see Appendix I.

Historical observations of storm surge, wave height, and period were collected during storms that impacted the HGA, and their maximum values were used to construct the CDFs for each data. A total of 30 storms that made landfall within approximately 400 km of the HGA from 1993 to 2022 were selected, which are listed in Table 2. Storm surge data were obtained from NOAA tide and current stations 8771341 (Galveston Bay Entrance, North Jetty, Texas) and 8771510 (Galveston Pleasure Pier, Texas), which are marked as T1 and T2 in Fig. 1, while significant wave height and mean zero-crossing wave period (T_z) were observed at NDBC station 42035 (22 NM East of Galveston, Texas), marked as W1 in Fig. 1. To ensure consistency in the wave period data, T_z was transformed to T_m using the empirical relationship $T_m \approx 1.1T_z$ (Chun and Suh 2018).

Table 2. List of selected historical storms

Year	Duration	Name
1993	18–21 June	Arlene
1995	30–31 July	Dean
1998	21–22 August	Charley
1998	7–13 September	Frances
1999	22–23 August	Bret
2001	4–6 June	Allison
2002	4–8 September	Fay
2002	22–26 September	Lili
2003	13–16 July	Claudette
2003	16 August	Erika
2003	30 August–1 September	Grace
2004	15–23 September	Ivan
2005	19–21 July	Emily
2005	22–25 September	Rita
2007	16 August	Erin
2007	12–13 September	Humberto
2008	22–24 July	Dolly
2008	5 August	Edouard
2008	3 September	Gustav
2008	11–14 September	Ike
2010	6–8 September	Hermine
2011	29 July	Don
2015	15–18 June	Bill
2017	21–23 June	Cindy
2017	25–30 August	Harvey
2019	19 September	Imelda
2020	24–26 July	Hanna
2020	26–27 August	Laura
2020	19 September	Beta
2021	13–14 September	Nicholas

The total volume of dune erosion was estimated by integrating the erosion rate q_D over the duration of each synthetic storm, which was computed at every time step using the time series of input variables (S, H_s, and T_m). While bias correction was available only to the extreme values of these variables, each entire time series must be bias-corrected for more accurate dune erosion predictions. For a rough correction, the time series data were adjusted by multiplying each value by the ratio ($r_{\max}$) of the bias-corrected extreme data to the non-bias-corrected extreme value for each storm as follows:

$$r_{\max} = \frac{\hat{x}_{m,p}}{x_{m,p}}, \quad \hat{x}_{m,p}(t) = r_{\max} \times x_{m,p}(t) \quad (9)$$

where $x_{m,p}(t)$ = non-bias-corrected time series data; and $\hat{x}_{m,p}(t)$ = bias-corrected time series data. Although such multiplicative scaling may introduce some distortion of physical storm characteristics, this approach provides a consistent adjustment during each storm event. An example of the time series data correction process is schematically illustrated in Fig. 3.

Alternative Approach: Copula Sampling

The aforementioned process for predicting dune erosion relies heavily on the properties of synthetic storm tracks, each of which represents a single, deterministic storm. To predict probabilistic dune erosion via an alternative, stochastic method, we developed a copula sampling approach. Since dune erosion analysis requires multiple input variables, a multivariate analysis is necessary to account for their dependency, despite each variable having its own marginal probability distributions. A copula is a multivariate CDF for variables that follow a uniform distribution, defined to describe the variables' joint probability distribution (Frees and Valdez 1998). In this study, each uniform variable corresponds to the marginal CDF of an input variable for the dune erosion model. The Archimedean copula was adopted to model the dependence structures among the random variables, using Clayton, Gumbel, and Frank copula generators (Genest and Rivest 1993). The dependence parameter of the generator was estimated using Kendall's τ correlation coefficient, which quantifies the dependence between samples of random variables by comparing the number of concordant and discordant pairs (Kendall 1938).

In this context, the bias-corrected extreme data of S, H_s, and T_m were represented as input random variables, and they were fitted to the GEV distribution to construct marginal CDFs, as was done for observed or modeled data. First, we generated independent uniform samples ($u_{i,j}$), which correspond to the CDFs of the input random variables X_i ($j = 1, 2, \ldots, N$, where N is the number of samples). Next, correlated uniform samples ($v_{i,j}$) were generated from $u_{i,j}$ using sampling algorithms based on the Archimedean copula (Melchiori 2006). Each set of $v_{i,j}$ was transformed into realizations of the correlated variable X_i by applying the inverse of the marginal CDF of X_i. These realizations of bias-corrected S, H_s, and T_m served as inputs for the dune erosion model. Since the wave incidence angle is stochastically random and not suitable for bias correction, ϕ was sampled directly from the CDFs of synthetic storm data. Wave incidence angles were collected at various nearshore locations from all synthetic storms, recorded at the time when peak S occurred (referred to ϕ_p), and the collected angles were fitted to a lognormal distribution. As with other

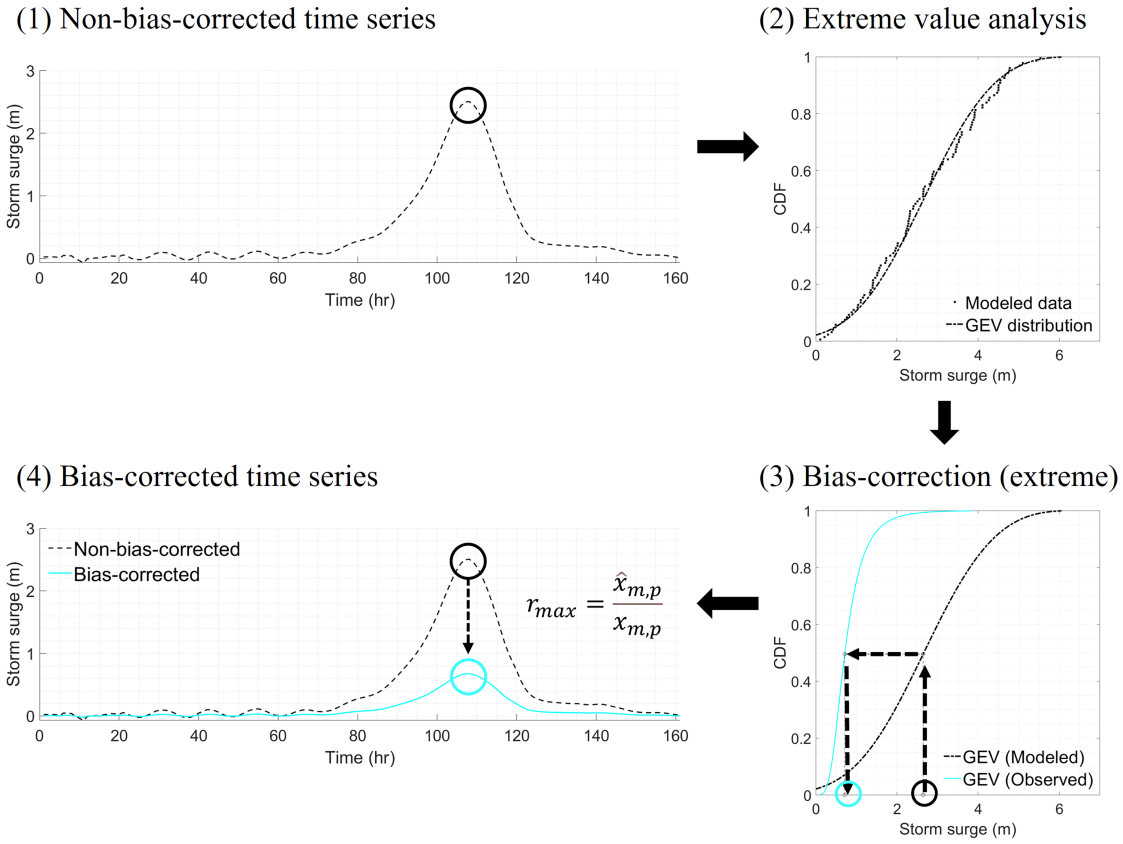

Fig. 3. Process for bias-correction of time series data.

input variables, independent uniform samples were generated and transformed into realizations of ϕ_p, which also served as the inputs for the dune erosion model.

While a storm duration was predetermined for each synthetic storm, it was stochastically predicted in the copula sampling approach. For this study, the coastal storm duration (D) was defined as the period during which the significant wave height exceeds the 95% percentile threshold (Davies et al. 2017; Martzikos et al. 2021), determined using hourly data observed at NDBC station 42035 from 1993 to 2023 (excluding 2022 due to a lack of data) within the Atlantic hurricane season (i.e., June 01–November 30). Fig. 4 displays the percentiles of observed significant wave heights, representing that the 95% percentile is 1.62 m in the study area. If consecutive storms were separated by less than 12 h, they were regarded as a single event (Li et al. 2014; Wahl et al. 2016; Martzikos et al. 2021). This threshold was used to determine D for both historical and synthetic storms. All 30 historical storms were simulated with hydrodynamic and wave models, and the maximum H_s from each storm was retrieved to determine D. The same procedure was done for synthetic storms. Both historical and synthetic storm durations were fitted to the lognormal distribution, along with the bias-corrected storm duration data itself. For more details on the fitting of D and ϕ_p to probability distributions, see Appendix I.

Dependence among S, H_s, T_m, and D was evaluated using bias-corrected data at various nearshore locations. A 4×4 matrix of Kendall's τ values was provided for each location, with an element $\tau_{i,j}$ representing the correlation between pairs of variables (X_i and X_j), where $\mathbf{X} = [X_1\ X_2\ X_3\ X_4]^T = [S\ H_s\ T_m\ D]^T$. Kendall's τ values ranged from 0.2 to 0.6 among S, H_s, and T_m, indicating strong correlations. Conversely, the coefficients between D and each of the

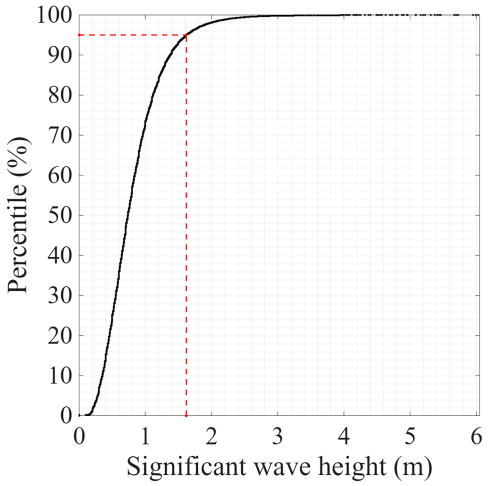

Fig. 4. Percentiles of significant wave heights observed at the NDBC station from 1993 to 2023.

other three variables were low or occasionally negative, suggesting little or no correlation. Therefore, D was treated as independent of S, H_s, and T_m for synthetic storms used in this study and was excluded from correlated copula sampling. Since copula sampling requires a single dependence parameter, the average of the three relevant coefficients (τ_{12}, τ_{13}, and τ_{23}) was used as the representative Kendall's τ to estimate dependence parameters, which were further averaged across all locations to determine the Archimedean copula's dependence parameter. This evaluation was conducted

Table 3. Estimates of the Archimedean copula's dependence parameter

Data type	Present	Future (low SLR)	Future (middle SLR)	Future (high SLR)
Nonparametric bias correction	1.895	1.807	1.790	1.783
Parametric bias correction	1.895	1.850	1.833	1.825

for every climate scenario, with the resulting estimates of dependence parameter present in Table 3.

While only extreme values were available for S, H_s, and T_m, full time series data for these variables were required to calculate erosion rate at each time step. To address this, we simplified and idealized time series of storm events, referred to as a storm archetype. Two archetype structures were assessed: one with a simple and linear profile (Storm archetype 1), and another with a nonlinear, asymmetric profile for more realistic storm-driven dynamics (Storm archetype 2). In Storm archetype 1, S, H_s, and T_m increase linearly to their extreme values during the first half of the storm duration D and decrease linearly back to initial values during the second half. In Storm archetype 2, H_s and T_m increase gradually up to $D/2$, and increase abruptly to their extremes by $2D/3$, before returning to initial values by D. S follows a similar pattern but with a lag relative to the waves. For both archetypes, storms begins and ends at zero storm surge ($S = 0$), a threshold value ($H_s = 1.62$ m) for significant wave height, and a normal nonstorm condition far offshore of Galveston ($T_m = 2.5$ s) for mean absolute wave period. Only storm waves are considered; remotely generated swell waves are ignored, as they are not dominant during storm events. Conceptual sketches of both storm archetypes are illustrated in Fig. 5.

To represent the nonlinear, time-varying wave incidence angle in storm archetypes, the wave angle time series $\phi(t)$ was modeled using a hyperbolic function as follows:

$$\phi(t) = \phi_p + \Delta\phi \tanh\left(\frac{t - t_p}{D_\phi}\right) \tag{10}$$

where $\Delta\phi$ = amplitude of wave angle variation; t_p = time at peak storm surge; and D_ϕ is a timescale. This model provided the best fit to the original ϕ time series during synthetic storms with $\Delta\phi = 30\,(^\circ)$ and $D_\phi = D/2$, and was used in both storm archetypes.

The overall process for the copula sampling approach is illustrated in Fig. 6, which was repeated with n sets of samples, generating n values of percent dune erosion.

Results and Discussion

Calibration of Transport Coefficient

The empirical transport coefficient C_s of the dune erosion model [in Eq. (1)] was determined by comparing modeled eroded volumes with estimates from the Coastal Texas Study for four historical hurricanes: Frances (1998), Allison (2001), Rita (2005), and Ike (2008). USACE's estimates were based on simulations conducted with the numerical model Storm-Induced Beach Change (SBEACH), and the simulated dune erosion profiles can be found in USACE Galveston District and GLO (2021c). For our study, these hurricanes were simulated in the hydrodynamic and wave models after converting their track data into spider web wind velocity and pressure fields, and then the output data of S, H_s, and T_m were used as inputs for the dune erosion model. The model tested values of C_s at 1.0×10^{-4}, 1.25×10^{-4},

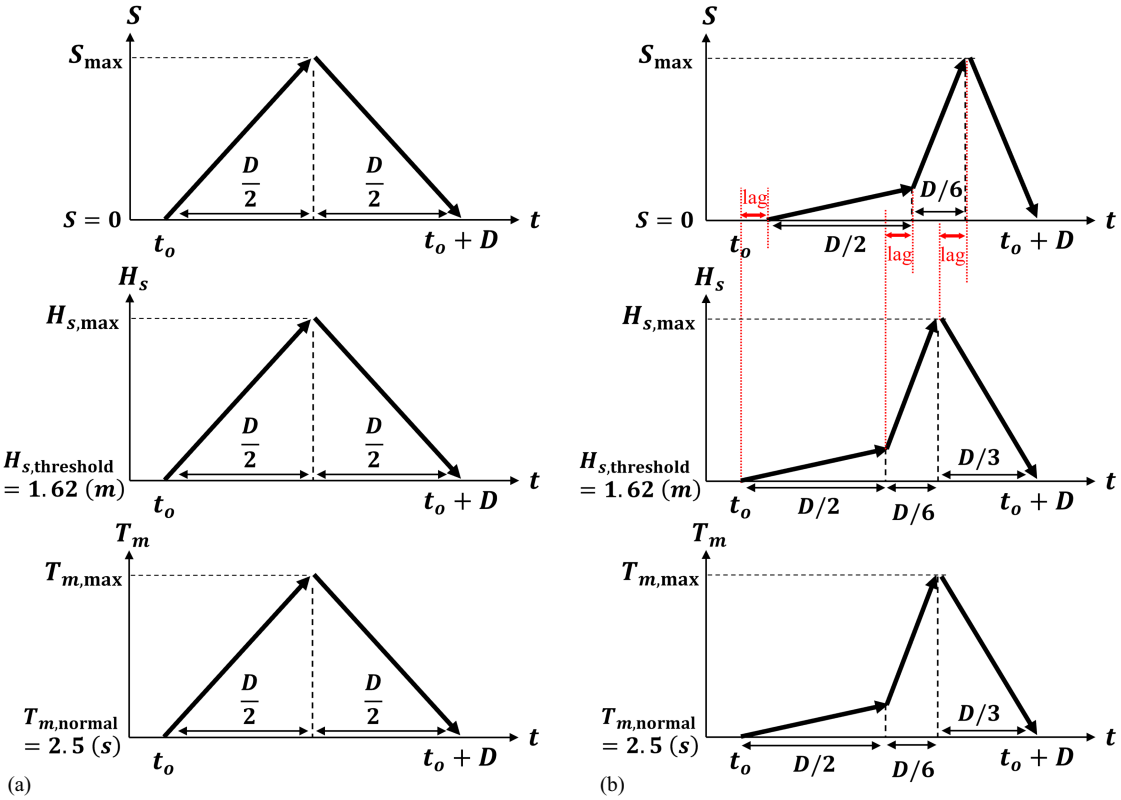

Fig. 5. Time series of S, H_s, and T_m for storm archetypes: (a) Archetype 1; and (b) Archetype 2.

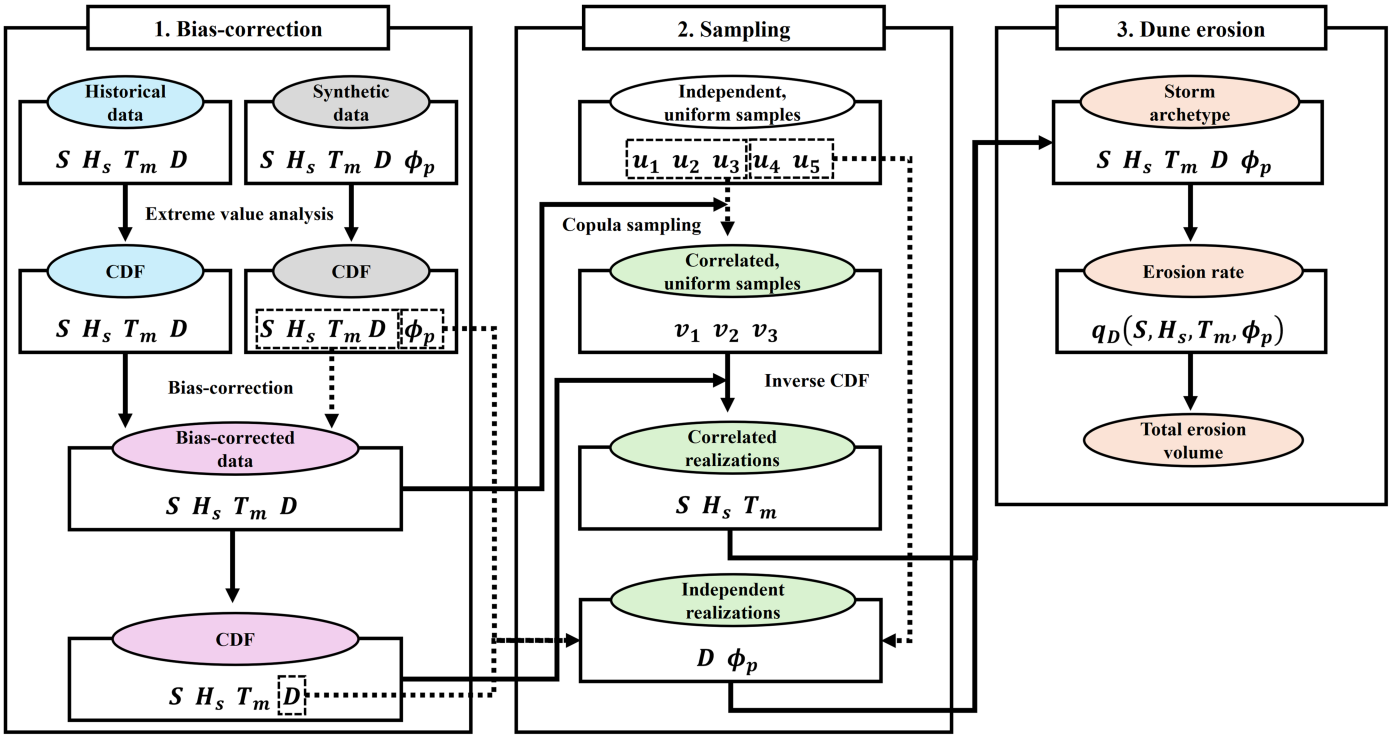

Fig. 6. Process for copula sampling approach.

Table 4. Estimations of dune erosion percent in the beach and dune system under different C_s

		Galveston Island				Bolivar Peninsula			
		Landward dune erosion		Seaward dune erosion		Landward dune erosion		Seaward dune erosion	
Transport coefficient, C_s	Hurricane	Overwash (%)	Backwash (%)	Overwash (%)	Backwash (%)	Overwash (%)	Backwash (%)	Overwash (%)	Backwash (%)
1×10^{-4}	Frances	0		32.11		0		19.81	
	(1998)	0	0	0.04	32.07	0	0	0	19.81
	Allison	0		8.50		0		15.74	
	(2001)	0	0	0	8.50	0	0	0	15.74
	Rita (2005)	0		54.64		0		36.66	
		0	0	0.11	54.53	0	0	0	36.66
	Ike (2008)	44.15		100		47.56		100	
		3.48	40.66	5.55	94.45	12.23	35.33	7.79	92.21
1.25×10^{-4}	Frances	0		40.13		0		24.77	
	(1998)	0	0	0.05	40.08	0	0	0	24.77
	Allison	0		10.63		0		19.67	
	(2001)	0	0	0	10.63	0	0	0	19.67
	Rita (2005)	0		68.30		0		45.83	
		0	0	0.13	68.16	0	0	0	45.83
	Ike (2008)	72.24		100		78.95		100	
		5.35	66.89	3.90	96.10	18.50	60.45	4.84	95.16
1.5×10^{-4}	Frances	0		48.16		0		29.72	
	(1998)	0	0	0.06	48.10	0	0	0	29.72
	Allison	0		12.75		0		23.61	
	(2001)	0	0	0	12.75	0	0	0	23.61
	Rita (2005)	0		81.95		0		54.99	
		0	0	0.16	81.80	0	0	0	54.99
	Ike (2008)	98.17		100		100		100	
		6.87	91.30	2.65	97.35	22.76	77.24	2.97	97.03

and 1.5×10^{-4}, calculating the percent dune erosion during each hurricane for different C_s values, as described in Table 4. The results showed that $C_s = 1.25 \times 10^{-4}$ provided the most accurate estimates for the HGA, with modeled percent dune erosion on Galveston Island and Bolivar Peninsula as follows: 40.13% and 24.77% during Frances, 10.63% and 19.67% during Allison, 68.30% and 45.83% during Rita, and both 100% during Ike. This empirical coefficient was adopted in the model for

J. Waterway, Port, Coastal, Ocean Eng., 2026, 152(4): 04026009

predicting dune erosion during synthetic storm scenarios, as well as in the copula sampling approach.

Bias Correction of S, H_s, and T_m

The extreme values of bias-corrected S, H_s, and T_m, collected at the historical measurement locations, were compared with those before applying the bias correction, along with the resulting percent dune erosion as shown in Fig. 7. Bias correction led to the decrease in storm surge values for both present and future climate conditions, while mean absolute wave period values increased. For significant wave height, the non-bias-corrected data were generally greater than the bias-corrected data, except at higher values (above approximately 5 m) and lower values (below approximately 2 m). On average, storm surge was reduced by 74%–75% and significant wave height by 23%–24% with bias correction, while mean absolute wave period increased by 23%–24% (Table 5). When comparing values across climate scenarios, S was higher under present-day conditions than in future scenarios, decreasing as SLR increased, for both non-bias-corrected and bias-corrected data. In contrast, H_s was greater in future scenarios and increased with SLR. T_m was higher in future scenarios but did not show a clear trend with SLR. These results demonstrate that storm surge is inversely dependent to local water depth, aligning with what is expected from a storm surge balance equation, even though future storms are more intense. Conversely, wave height and period are more directly influenced by storm intensity and less affected by water level or depth compared to storm surge.

Fig. 8 presents one-to-one comparisons of bias-corrected values and resulting percent dune erosion between nonparametric and parametric methods. While both methods produced similar bias-corrected data for S, H_s, and T_m at lower values, the parametric method provided higher predictions for H_s in the present climate and for T_m in both present and future climate scenarios at higher values. The parametric QM and QDM approaches rely on the behavior of the probability distribution function, particularly in the upper tail. Although the GEV distribution is well-suited for modeling extreme values, the uncertainty in its upper tail, caused by the limited number of observed extremes, can lead to excessive predictions for wave parameters. Despite these differences, both nonparametric and parametric methods yielded comparable results for percent dune erosion, which implies that storm-driven dune erosion is more sensitive to extreme storm surge than to wave parameters. This observation is supported by Fig. 7, where the application of bias correction reduced percent dune erosion in alignment with decreases in storm surge. In addition, percent dune erosion increased under higher SLR scenarios, suggesting that the sea level contributions (storm surge and mean sea level) are crucial in coastal erosion processes.

Probabilistic dune erosion was predicted using the annual exceedance probability (AEP), determined based on the nonexceedance probability per storm and storm frequency (λ)

$$\mathrm{AEP} = 1 - F_m^{\lambda}, \quad F_m = 1 - \frac{m - 0.4}{n + 1 - 0.8} \tag{11}$$

where F_m = estimated nonexceedance probability (or CDF) at rank m out of n data points (Gringorten 1963). Storm frequency for the present scenario was determined as 1 storm per year (30 historical storms over 30 years). For future scenarios, it was adjusted by multiplying the present value of λ by the ratio of the number of synthetic storms in future to present, resulting in $\lambda = 158/115 = 1.374$ storms per year. The predictions of probabilistic percent dune erosion with respect to AEP are presented in Fig. 9. The annual-average dune erosion, which is equivalent to the area under the probabilistic dune erosion curve, was estimated by integrating the probabilistic dune erosion over the range of AEPs, as presented in Table 6.

The results show that bias correction led to a significant reduction in percent dune erosion for any climate scenario, regardless of where a nonparametric or parametric method was used. Without bias correction, annual-average percent dune erosion exceeded 30% under the present climate condition and 60% under future conditions. These values are unrealistic when considering current and projected storm intensity and frequency and not feasible for coastal protection planning against storm surge. Otherwise, bias-corrected predictions were 8%–9% for the present and 32%–40% for future conditions, which better reflected the anticipated storm activity and projected SLR. The necessity of applying bias correction to GCM-based synthetic storm data is supported by the pronounced difference between these results, particularly for hydrodynamic and wave parameters, not only to ensure statistical consistency with the historical observations itself but also to prevent overestimation of future coastal processes or risk and to improve prediction accuracy.

In general, the parametric method yielded comparable but marginally higher probabilistic dune erosion than the nonparametric method at the same AEP across all climate scenarios, leading to a slightly greater annual-average percent dune erosion with the parametric method. As a measure of uncertainty in dune erosion predictions based on bias-corrected synthetic storm data, these

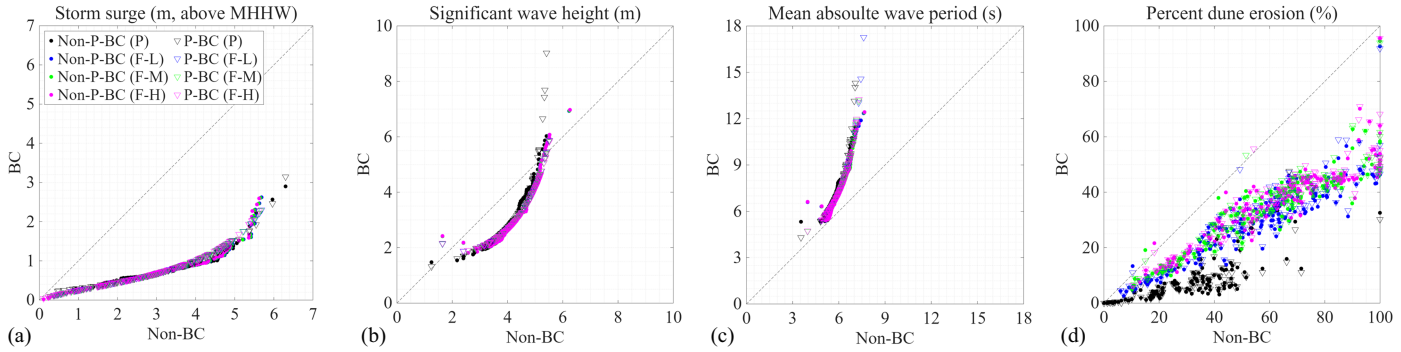

Fig. 7. Comparison of extreme non-BC and BC data: (a) storm surge (S); (b) significant wave height (H_s); (c) mean absolute wave period (T_m); and (d) percent dune erosion. Non-P-BC = nonparametric bias correction; P-BC = parametric bias correction; P = present climate; F = future climate; and L, M, and H = low, middle, and high SLR scenarios, respectively.

J. Waterway, Port, Coastal, Ocean Eng., 2026, 152(4): 04026009

Table 5. Mean values of non-BC and BC data of S, H_s, and T_m

Data type	Present	Future (low SLR)	Future (middle SLR)	Future (high SLR)
S (m, above MHHW)				
Non-BC	3.157	2.853	2.842	2.819
Nonparametric BC	0.785	0.710	0.707	0.701
Parametric BC	0.819	0.744	0.741	0.735
H_s (m)				
Non-BC	4.022	4.263	4.268	4.278
Nonparametric BC	3.036	3.217	3.221	3.229
Parametric BC	3.108	3.271	3.275	3.282
T_m (s)				
Non-BC	5.756	5.937	5.944	5.943
Nonparametric BC	7.066	7.299	7.307	7.304
Parametric BC	7.137	7.372	7.380	7.377

two results effectively provided lower and upper bounds for the estimate. Under the present scenario, the dual-dune system was predicted to be eroded by 8.46%–8.74% of its total volume, while future scenarios estimated erosion of 32.97%–34.01%, 37.67%–38.32%, and 39.75%–40.64% for low, middle, and high SLR scenarios, respectively.

Assessment of Storm Archetypes

Storm archetypes were assessed for their accuracy in predicting dune erosion by calculating percent dune erosion for 115 present-day synthetic storms. This analysis was conducted using both non-bias-corrected and bias-corrected data sets, and the results were compared to those obtained from synthetic storms' full time series data. Fig. 10 presents a one-on-one comparison for each storm, showing good agreement between the two approaches in lower percent dune erosion, but greater scatter at higher values, especially for the non-bias-corrected data. Storm archetype 1 tended to overestimate dune erosion with bias-corrected data under severe storms compared to the full time series approach, while Archetype 2 consistently underestimated dune erosion for both non-bias-corrected and bias-corrected data.

A similar trend was observed in the probabilistic dune erosion curves (Fig. 11). With non-bias-corrected data, storm archetypes predicted lower probabilistic dune erosion than the full time series approach, resulting in annual-average percent dune erosion of 29.68% for Archetype 1 and 17.47% for Archetype 2. For bias-corrected data, Archetype 1 predicted higher percent dune erosion than the full time series approach at lower AEPs, while marginally lower at higher AEPs, leading to comparable annual-average dune erosion values: 8.68% and 9.40% for nonparametric and parametric methods, respectively. Otherwise, Archetype 2 yielded values of 5.01% and 5.58%, which were considerably lower than predictions from the full time series approach. This supports that, although Storm Archetype 2 can closely predict probabilistic dune erosion under severe storms, it is not suitable for predicting dune erosion, given the study's focus on annual-average values derived from bias-corrected data. Therefore, Archetype 1 was selected for further use in the copula sampling approach.

Analysis: Copula Sampling Approach

Fig. 12 compares the observed and sampled (or bias-corrected) joint CDFs of S, H_s, and T_m on the copula scale for the present climate scenario. The close alignment with the 1:1 line was observed, indicating that the copula sampling approach reproduced the observed multivariate dependence structure well, which is important for accurate dune erosion prediction. Minor scatter around the diagonal reflects sampling variability attributed to the limited number of observed data points.

An optimal sample size n for the copula sampling approach was identified as the minimum size at which the mean annual-average dune erosion stabilized with low variance. Specifically, sample sizes with a coefficient of variation (CV) less than 0.05 were considered sufficiently reliable. Sample sizes of 100, 200, 500, 1,000, 2,000, and 5,000 were tested by estimating a single annual-average percent dune erosion, repeating this process 1,000 times, thereby generating 1,000 values of annual-average percent dune erosion for each sample size. Based on these results, $n = 1{,}000$ was adopted as the optimal sample size for the subsequent copula sampling approach in this study (see Appendix II for more details on sample size optimization).

Fig. 13 illustrates probabilistic percent dune erosion curves yielded by the copula sampling approach with different copula generators and bias-correction methods, along with 95% confidence intervals (CIs). The lower and upper bounds of the 95% CIs correspond to the 2.5th and 97.5th percentiles of the 1,000 probabilistic percent dune erosion values for every AEP (i.e., 976th and 25th ranked values out of 1,000). For the present scenario, probabilistic dune erosion predictions aligned with those from the full time series approach at high AEPs but are higher at low AEPs, leading to a greater annual-average dune erosion ranging 9.09%–9.60% for nonparametric and 9.46%–10.08% for parametric methods (Table 7). The full time series approach is deterministic and limited by the number of available synthetic storms, which may not capture rare, severe storm events such as Hurricane Ike, which cause extreme dune erosion. Therefore,

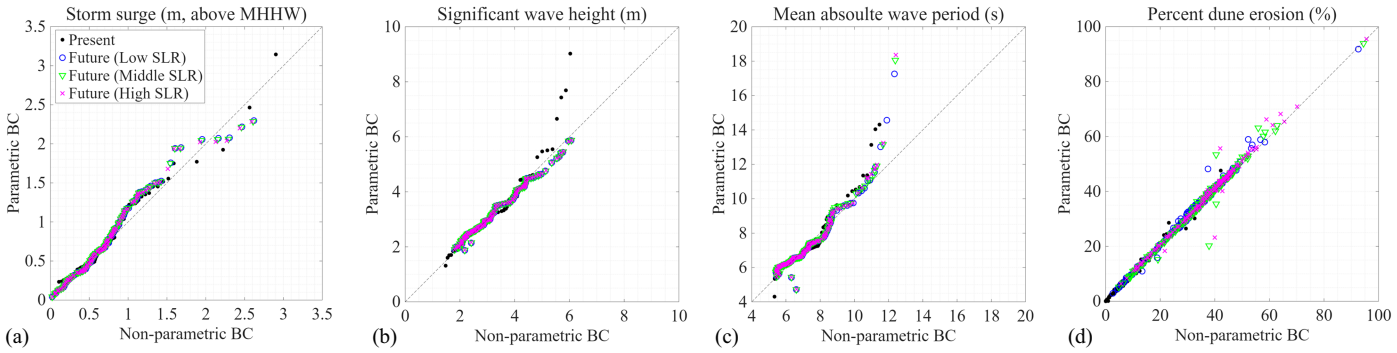

Fig. 8. Comparison of the results of nonparametric BC and parametric BC: (a) storm surge (S); (b) significant wave height (H_s); (c) mean absolute wave period (T_m); and (d) percent dune erosion.

J. Waterway, Port, Coastal, Ocean Eng., 2026, 152(4): 04026009

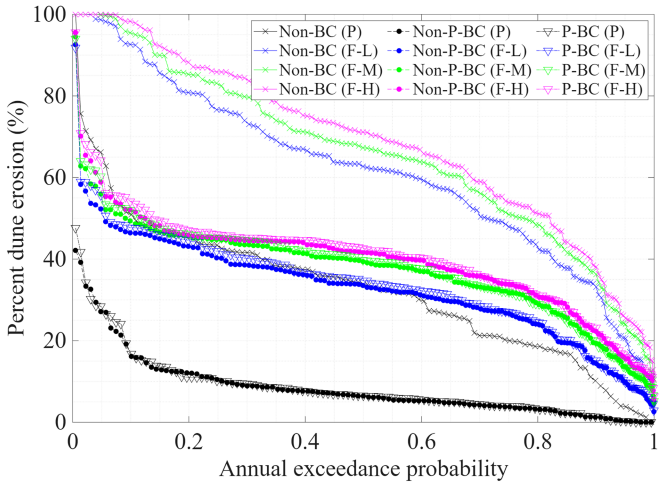

Fig. 9. Probabilistic dune erosion percent with respect to AEPs, predicted by the full time series approach. Abbreviations are the same as Fig. 7.

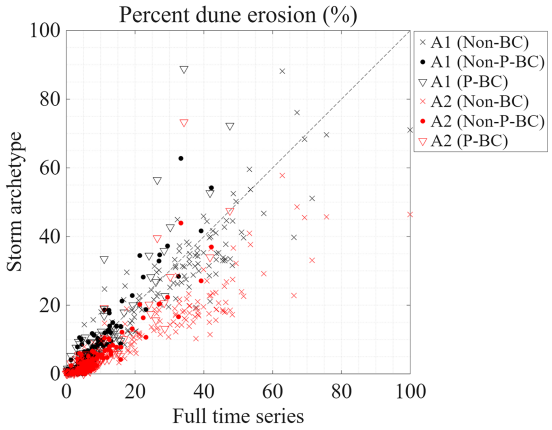

Fig. 10. One-on-one comparison of percent dune erosion estimated using full time series data and storm archetypes. A1 = Archetype 1; A2 = Archetype 2.

Table 6. Annual-average percent dune erosion using non-BC and BC data

Data type	Present (%)	Future (low SLR) (%)	Future (middle SLR) (%)	Future (high SLR) (%)
Non-BC	32.91	61.78	65.89	68.86
Nonparametric BC	8.46	32.97	37.67	39.75
Parametric BC	8.74	34.01	38.32	40.64

this approach cannot fully reflect the impact of severe storms. In contrast, the copula sampling approach is stochastic, generating a large number of samples that can account for both severe dune erosion at low AEPs and minimal impacts at high AEPs. This pattern was observed in future scenarios as well: the copula sampling approach predicted higher probabilistic dune erosion at low AEPs and lower erosion at high AEPs compared to the full time series approach. Nonetheless, both approaches provided consistent annual-average dune erosion predictions under future climate change: 33.57%–35.70%, 35.90%–37.96%, and 37.69%–39.75% using the copula approach for low, middle, and high SLRs, respectively.

Based on the dune erosion prediction results, sensitivity to both copula generator choice and bias-correction method was analyzed. For the present scenario, the Gumbel copula presented the highest probabilistic dune erosion at lower AEPs, followed by Clayton, and the lowest with Frank, but this order reversed at higher AEPs, leading to the annual-average dune erosion being highest with Frank and lowest with Gumbel. In future scenarios, the Frank copula consistently predicted the highest dune erosion, followed by Clayton, and the lowest with Frank across the AEPs, resulting in the same pattern in annual-average dune erosion. Consequently, Clayton copula is regarded as the most suitable copula generator, as it provides moderate predictions among three copulas. Regardless of copula type, predicted dune erosion was consistently higher with the parametric method than the nonparametric method. For the present scenario, predictions were more robust to the choice of a bias-correction method than to copula generator type, but more robust to the choice of the copula generator in the future scenarios.

The 95% CIs accounted for the uncertainty in the copula sampling approach in this study. For both climate scenarios, the CIs

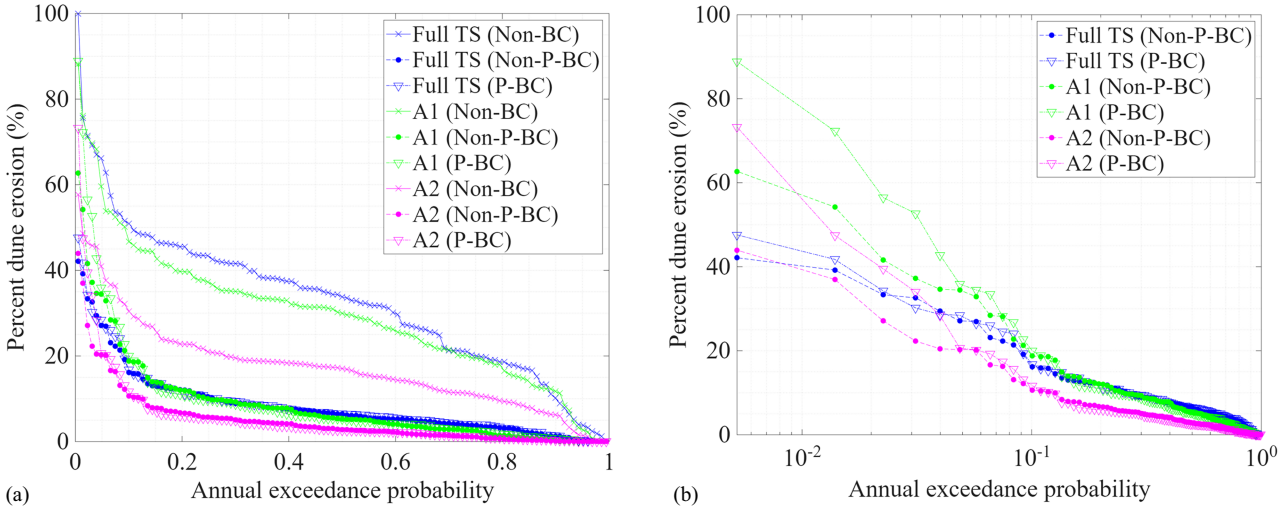

Fig. 11. Probabilistic percent dune erosion with respect to AEPs under the present climate scenario, predicted using full TS approach and storm archetypes: (a) linear-scale *x*-axis; and (b) log-scale *x*-axis with bias-corrected results.

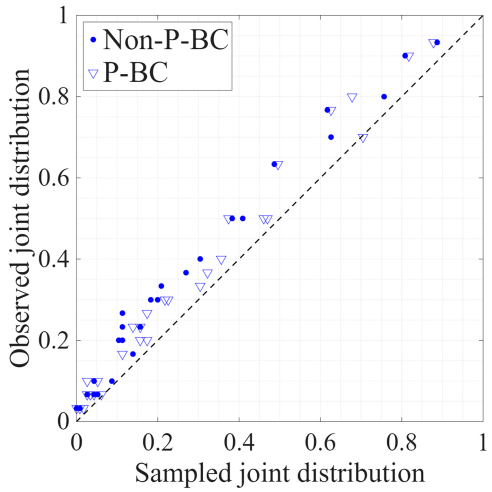

Fig. 12. Comparison of observed and sampled joint distributions on the copula scale for the present climate scenario.

were wider at lower AEPs than at higher AEPs (Fig. 13), indicating greater uncertainty associated with severe dune erosion events. Since pronounced erosion is rare under current sea level and storm conditions, considerable uncertainty appears at lower AEPs in the present scenario. For future scenarios, however, uncertainty at lower AEPs is relatively minor, particularly in higher SLR scenarios, as intensified storms and increased mean sea level are more likely to cause complete erosion, leading to more certain predictions. Conversely, the annual-average percent dune erosion exhibited different trends in CI ranges. The overall CI ranges (i.e., from the lowest lower bound to the highest upper bound) within a climate scenario is 8.32–10.87 for the present climate and 32.03–37.31, 34.25–39.66, and 35.94–41.36 for low, middle, and high SLR scenarios of the future climate, respectively. This implies that, despite reduced uncertainty for individual severe events, prediction in future dune erosion still remains challenging overall due to the anticipated higher frequency of severe storms in the future.

Comparison with the Coastal Texas Project Plan

According to the Coastal Texas Study (USACE Galveston District and GLO 2021b), the average rebuild frequency of the beach and dune system was estimated to be a 5- to 8-year cycle, depending on the SLR scenario. To be specific, it was 7–8 years under low SLR, 6–7 years under middle SLR, and 5–7 years under high SLR. USACE's SLR scenarios increased over the project service life from 2035 to 2085, ranging from approximately 0.23 to 0.53 m for low SLR, 0.29 to 0.78 m for middle SLR, and 0.43 to 1.51 m for high SLR, relative to the year 2000. The limit state for dune restoration was defined as a 50% reduction in dune height, which corresponds to approximately 80% erosion of the dual-dune system.

It is important to note that this study aims to provide conservative predictions of dune erosion by focusing on storm-driven instantaneous erosion, rather than long-term recovery processes or poststorm return flows. The analysis was designed to estimate erosion during storm impacts, without simulating full life cycle dune nourishment. Consequently, such estimates led to a linear deterioration of the dune, representing the conservative but necessary amount of dune nourishment required, rather than actual nourishment design practices.

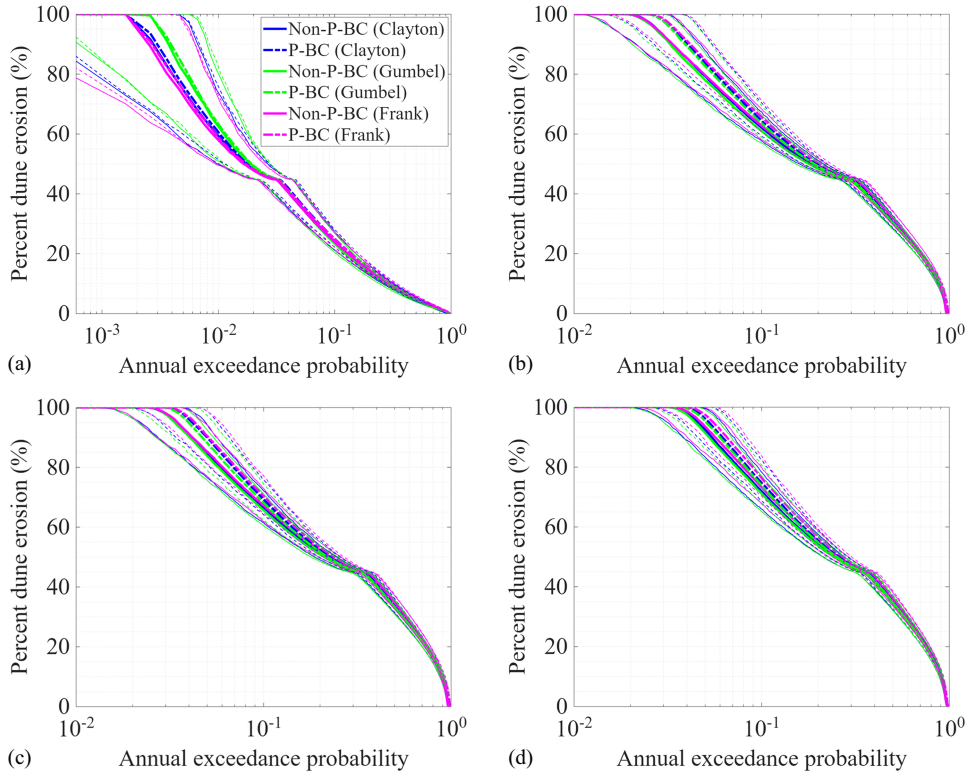

Fig. 13. Probabilistic percent dune erosion with respect to AEPs, predicted by copula sampling approach. Bold lines are mean values, and thin lines are 95% CIs at each AEP: (a) present scenario; (b) future scenario with low SLR; (c) future scenario with middle SLR; and (d) future scenario with high SLR.

Table 7. Means and standard deviations of 1,000 annual-average percent dune erosion using copula sampling approach

Scenario	Copula generator	Bias correction	Mean (95% CI) (%)	Standard deviation (%)
Present	Clayton	Nonparametric	9.32 (8.56–10.15)	0.413
		Parametric	9.75 (8.94–10.60)	0.405
	Gumbel	Nonparametric	9.09 (8.32–9.94)	0.411
		Parametric	9.46 (8.68–10.29)	0.396
	Frank	Nonparametric	9.60 (8.82–10.38)	0.390
		Parametric	10.08 (9.34–10.87)	0.399
Future (low SLR)	Clayton	Nonparametric	33.86 (32.36–35.35)	0.794
		Parametric	34.70 (33.21–36.30)	0.806
	Gumbel	Nonparametric	33.57 (32.03–35.13)	0.794
		Parametric	34.46 (32.91–36.07)	0.814
	Frank	Nonparametric	34.78 (33.10–36.42)	0.830
		Parametric	35.70 (34.22–37.31)	0.803
Future (middle SLR)	Clayton	Nonparametric	36.12 (34.57–37.80)	0.812
		Parametric	37.06 (35.61–38.76)	0.825
	Gumbel	Nonparametric	35.90 (34.25–37.52)	0.837
		Parametric	36.72 (34.99–38.35)	0.844
	Frank	Nonparametric	37.01 (35.43–38.78)	0.859
		Parametric	37.96 (36.35–39.66)	0.848
Future (high SLR)	Clayton	Nonparametric	37.84 (36.05–39.43)	0.882
		Parametric	38.78 (37.15–40.49)	0.855
	Gumbel	Nonparametric	37.69 (35.94–39.43)	0.896
		Parametric	38.54 (36.86–40.19)	0.852
	Frank	Nonparametric	38.82 (37.13–40.52)	0.863
		Parametric	39.75 (38.00–41.36)	0.846

Based on the annual-average percent dune erosion predicted by the full time series approach (Table 6), the dune restoration cycle is demanded to be approximately 9.5 years under the present climate condition. Using the copula sampling approach (Table 7), it is predicted as 8–9 years, which aligns well with the full time series results. For future scenarios, both approaches consistently indicate that dune rehabilitation will be needed every 2–2.5 years. Compared to USACE's estimates, this study's dune erosion predictions are broadly consistent with the Coastal Texas Study's dune nourishment plan, demonstrating the applicability of the semiempirical analytical dune erosion model to the beach and dune system.

The annual-average percent dune erosion suggests that, under the present climate condition, the beach and dune system would provide effective flood defense against storm surges in the long term. However, in future scenarios, considerable erosion of the dune system is projected substantially increasing flood risk for coastal communities. Hence, even if the current plan for the beach and dune system remains a viable countermeasure to storm surge in the present day, a more reliable coastal barrier is recommended for the future. Raising the dune crest height would involve higher initial construction costs, but it would likely extend the interval between dune rehabilitations and reduce long-term maintenance and management costs, as well as enhance safety for coastal communities. Alternatively, core-enhanced dunes or hybrid coastal structures, with a hard core and a sand outer layer, would be able to provide robust coastal defense and reduce the required volume of sand restoration, as suggested by Merrell et al. (2021). Furthermore, comparison of percent dune erosion across future scenarios indicates that several SLR projections lead to significant differences in dune erosion. Even with high SLR, the lower portion of the seaward dune is expected to be submerged by the increased mean sea level, due to its lower dune toe elevation. This study proposes that the Coastal Texas Project design be adjusted in response to sea level changes.

Conclusions

This study evaluated the feasibility of Coastal Texas Project beach and dune system by applying a semiempirical analytical model to predict dune erosion in the face of climate change. Synthetic storms were simulated with hydrodynamic, wave, and hurricane models to represent present and future storm climatology, and several SLR projections were incorporated into future climate scenarios. Their output data of storm surge, significant wave height, and mean absolute wave period were bias-corrected and then used as inputs for the dune erosion model. Probabilistic dune erosion was predicted for different climate scenarios, and the annual-average dune erosion was determined by integrating the probabilistic dune erosion over the range of AEPs. As a result, the annual-average percent dune erosion was predicted as approximately 8%–10% of dune volume under the present scenario, which corresponds to a dune rehabilitation cycle of about 8–10 years. Such a result closely aligns with the rebuild frequency plan for the Coastal Texas Project and supports the applicability of the dune erosion model to the beach and dune system. In future scenarios, however, the annual-average percent dune erosion increases to 33%–40%, requiring dune rehabilitation every 2–2.5 years, which would raise serious concerns on the long-term feasibility of the current plan. Consequently, while the proposed design is effective as a flood defense under the present condition, substantial modifications will be necessary to ensure coastal community safety in the future, such as raising dune crest heights or utilizing core-enhanced dunes or hybrid coastal structures, depending on sea level rise.

Bias correction was a key element of this study, ensuring statistical consistency between historical observations and model outputs. Particularly, QM was applied to present data sets and QDM to future data sets in both nonparametric and parametric ways. The use of bias-corrected data resulted in significant decreases in storm surge height and significant wave height, while increased mean

absolute wave period compared to non-bias-corrected data, leading to annual-average percent dune erosion reductions across all climate scenarios. These findings emphasize the critical role of bias correction to the storm and wave parameters, not only for statistical consistency but also for the feasibility and accuracy of coastal process and risk assessments. However, bias correction using parametric QM or QDM was found to be highly sensitive to the shapes and alignments of the CDFs for observed and GCM-based modeled data, especially on an upper tail. Therefore, conducting sensitivity analyses using multiple GCMs is needed for more robust and reliable outcomes.

Furthermore, we developed a copula sampling approach that incorporates synthetic storm data into the Archimedean copula framework to stochastically predict dune erosion. Bias-corrected data were used to generate correlated samples based on their CDFs and dependence parameters, which were then transformed into realizations of correlated input variables for the dune erosion model. These inputs created storm archetypes under several assumptions, enabling estimation of the total erosion over the storm duration. The accuracy of the storm archetype was validated by comparing its predictions to those from the synthetic storms' full time series data. The copula approach yielded the predictions comparable to those from the full times series data, both for the present and future scenarios. A minor difference arose from the copula approach's ability to account for extremely low probability events, which were not represented in limited synthetic storm data. The accuracy of the copula sampling approach for predicting dune erosion in the face of climate change is demonstrated, supporting its application for future coastal risk assessment and management.

Nevertheless, the current study entails several limitations. For the purpose of conservation prediction, poststorm processes were not explicitly modeled, including poststorm profile recovery and return flows, which are known to be crucial for long-term beach and dune evolution. The omission of these processes may lead to overprediction of dune erosion and higher estimated frequency of dune rehabilitation. In addition, longshore processes, which are also important when estimating storm-induced coastal dune erosion (Krafft et al. 2025), were not explicitly considered within the scope of this study. Although the combined effects of wind and infragravity (IG) waves were implicitly included through calibration of the empirical transport coefficient, the individual contributions of these components cannot be separated within the present modeling framework, as SWAN does not explicitly resolve IG waves. Furthermore, due to the limited sample sizes of extreme data, especially in the historical observations, the probability distributions of surge and wave parameters, as well as the dependence structure among these variables, remain uncertain. Despite these limitations, the proposed framework is appropriate to comparing climate scenarios and informing dune restoration planning. Addressing these limitations will be an important focus of future work.

Appendix I. Fitting to Probability Distributions

For parametric QM and QDM methods, both observed and modeled data were fitted to several probability distributions. Observed data were collected from 30 historical storms listed in Table 2, while modeled data were retrieved from 115 synthetic storms under present climate and 158 storms under future climate for each SLR scenario. Extreme values of S, H_s, and T_m were fitted to Gumbel, Weibull, and GEV distributions; D was fitted to lognormal, Gamma, and Weibull distributions using only nonzero duration values. The overall probability distribution for D was then adjusted to account for the discrete probability of zero-duration occurrences (Bedient et al. 2019). Modeled data of ϕ was fitted to lognormal, Gamma, and Weibull distributions at different locations, with the resulting CDFs used directly in the copula sampling approach for each climate scenario. Goodness of fit to the distributions was evaluated by the Akaike Information Criterion (AIC; Akaike 1974); the distribution with the smallest AIC was adopted. As summarized in Table 8, GEV distribution was adopted for S, H_s, and T_m, while lognormal distribution was used for D and ϕ.

Appendix II. Optimization of Sample Size

Table 9 presents the mean and CV values across all sample sizes under the present scenario, providing the CV values less than 0.05 with sample sizes of 1,000, 2,000, and 5,000.

Table 8. AICs of probability distributions for the observed (historical storms) and modeled (synthetic storms) data of variables

			Synthetic storm			
Variable	Distribution	Historical	Present	Future (low SLR)	Future (middle SLR)	Future (high SLR)
S	Gumbel	30.18	399.51	567.53	566.27	563.84
	Weibull	36.43	385.52	553.74	552.47	550.06
	GEV	30.52	387.27	550.62	549.31	546.81
H_s	Gumbel	85.02	298.83	394.54	394.88	395.70
	Weibull	91.74	248.80	342.23	342.54	343.27
	GEV	86.13	249.30	348.69	349.05	349.92
T_m	Gumbel	102.99	223.12	294.77	295.65	292.15
	Weibull	116.16	194.13	295.33	293.51	291.70
	GEV	104.25	184.24	272.65	272.70	269.03
D	Lognormal	241.18	786.74	1,150.67	1,150.54	1,139.37
	Gamma	243.61	803.54	1,150.44	1,150.34	1,146.21
	Weibull	245.55	834.52	1,192.34	1,192.30	1,191.38
ϕ_p (mean value)	Lognormal	—	927.77	1,367.30	1,370.34	1,374.05
	Gamma	—	940.00	1,384.58	1,386.21	1,388.29
	Weibull	—	940.88	1,379.72	1,381.15	1,383.47

Table 9. Means and CVs of 1,000 annual-average percent dune erosion using copula sampling approach at varying sample sizes for the present scenario

		Nonparametric			Parametric		
Sample size, n	Statistical metrics	Clayton	Gumbel	Frank	Clayton	Gumbel	Frank
100	Mean	9.30%	9.09%	9.64%	9.75%	9.47%	10.10%
	CV	0.141	0.140	0.130	0.135	0.134	0.127
200	Mean	9.33%	9.11%	9.60%	9.74%	9.47%	10.11%
	CV	0.098	0.101	0.094	0.096	0.096	0.088
500	Mean	9.29%	9.07%	9.63%	9.73%	9.47%	10.07%
	CV	0.063	0.063	0.060	0.062	0.062	0.057
1,000	Mean	9.32%	9.09%	9.60%	9.75%	9.46%	10.08%
	CV	0.044	0.045	0.041	0.041	0.042	0.040
2,000	Mean	9.29%	9.08%	9.60%	9.72%	9.45%	10.06%
	CV	0.031	0.031	0.029	0.029	0.031	0.028
5,000	Mean	9.30%	9.08%	9.60%	9.73%	9.48%	10.08%
	CV	0.020	0.020	0.018	0.019	0.020	0.017

Data Availability Statement

Some data, models, or code that support the findings of this study are available from the corresponding author upon reasonable request. Some data, models, or code generated or used during the study are proprietary or confidential in nature and may only be provided with restrictions.

Acknowledgments

This research was funded by NSF award nos. 2228485 and 2228486 under the program Strengthening American Infrastructure (SAI). The authors thank Prof. Kerry Emanuel for providing synthetic tropical cyclone track data sets from WindRiskTech.

Author Contributions

Seokmin Son: Conceptualization, Data curation, Formal analysis, Investigation, Methodology, Software, Validation, Visualization, Writing—original draft, Writing—review and editing; Meri Davlasheridze: Funding acquisition, Project administration, Writing—review and editing; Ashley D. Ross: Funding acquisition, Project administration, Writing—review and editing; Jeremy D. Bricker: Conceptualization, Funding acquisition, Project administration, Resources, Supervision, Writing—review and editing.

References

Akaike, H. 1974. "A new look at the statistical model identification." *IEEE Trans. Autom. Control* 19 (6): 716–723. https://doi.org/10.1109/TAC.1974.1100705.

Bedient, P. B., W. C. Huber, and B. E. Vieux. 2019. *Hydrology and floodplain analysis*. 6th ed. New York: Pearson.

Bruun, P. 1962. "Sea-level rise as a cause of shore erosion." *J. Waterway and Harb. Div.* 88 (1): 117–130. https://doi.org/10.1061/JWHEAU.0000252.

Bunya, S., et al. 2010. "A high-resolution coupled riverine flow, tide, wind, wind wave, and storm surge model for southern Louisiana and Mississippi. Part I: Model development and validation." *Mon. Weather Rev.* 138 (2): 345–377. https://doi.org/10.1175/2009MWR2906.1.

Callaghan, D. P., P. Nielsen, A. Short, and R. Ranasinghe. 2008. "Statistical simulation of wave climate and extreme beach erosion." *Coastal Eng.* 55 (5): 375–390. https://doi.org/10.1016/j.coastaleng.2007.12.003.

Cannon, A. J., S. R. Sobie, and T. Q. Murdock. 2015. "Bias correction of GCM precipitation by quantile mapping: How well do methods preserve changes in quantiles and extremes?" *J. Clim.* 28 (17): 6938–6959. https://doi.org/10.1175/JCLI-D-14-00754.1.

Carter, R. W. G. 1991. "Near-future sea level impacts on coastal dune landscapes." *Landscape Ecol.* 6 (1–2): 29–39. https://doi.org/10.1007/BF00157742.

Chun, H., and K.-D. Suh. 2018. "Estimation of significant wave period from wave spectrum." *Ocean Eng.* 163: 609–616. https://doi.org/10.1016/j.oceaneng.2018.06.043.

Ciavola, P., O. Ferreira, A. Van Dongeren, J. V. de Vries, C. Armaroli, and M. Harley. 2015. "Prediction of storm impacts on beach and dune systems." In *Hydrometeorological hazards: Interfacing science and policy*, edited by P. Quevauville, 227–252. Hoboken, NJ: Wiley.

Cid, A., T. Wahl, D. P. Chambers, and S. Muis. 2018. "Storm surge reconstruction and return water level estimation in Southeast Asia for the 20th century." *J. Geophys. Res.: Oceans* 123 (1): 437–451. https://doi.org/10.1002/2017JC013143.

Cooper, W. S. 1958. *Coastal sand dunes of Oregon and Washington*. New York: Geological Society of America.

Corbella, S., and D. D. Stretch. 2012. "Predicting coastal erosion trends using non-stationary statistics and process-based models." *Coastal Eng.* 70: 40–49. https://doi.org/10.1016/j.coastaleng.2012.06.004.

Davidson-Arnott, R. G. D. 2005. "Conceptual model of the effects of sea level rise on sandy coasts." *J. Coastal Res.* 216 (6): 1166–1172. https://doi.org/10.2112/03-0051.1.

Davies, G., D. P. Callaghan, U. Gravois, W. Jiang, D. Hanslow, S. Nichol, and T. Baldock. 2017. "Improved treatment of non-stationary conditions and uncertainties in probabilistic models of storm wave climate." *Coastal Eng.* 127: 1–19. https://doi.org/10.1016/j.coastaleng.2017.06.005.

Dean, R. G., and R. A. Dalrymple. 1991. *Water wave mechanics for engineers and scientists*. Singapore: World Scientific.

Deltares. 2024a. *D-flow flexible mesh. Computational cores and user interface. User manual*. Delft, Netherlands: Deltares.

Deltares. 2024b. *Delft3D-wave. Simulation of short-crested waves with SWAN. User manual*. Delft, Netherlands: Deltares.

de Schipper, M. A., B. C. Ludka, B. Raubenheimer, A. P. Luijendijk, and T. A. Schlacher. 2021. "Beach nourishment has complex implications for the future of sandy shores." *Nat. Rev. Earth Environ.* 2: 70–84. https://doi.org/10.1038/s43017-020-00109-9.

Dewitz, J. 2023. *National land cover database (NLCD) 2021 products: U.S. Geological Survey Data Release*. Sioux Falls, SD: Earth Resources Observation and Science (EROS) Center.

Ebersole, B. A., T. C. Massey, J. A. Melby, N. C. Nadal-Caraballo, D. L. Hendon, T. W. Richardson, and R. W. Whalin. 2018. *Ike Dike concept for reducing hurricane storm surge in the Houston Galveston region*. Final Rep. Jackson, MS: Jackson State Univ.

Emanuel, K. 2005. "Increasing destructiveness of tropical cyclones over the past 30 years." *Nature* 436 (7051): 686–688. https://doi.org/10.1038/nature03906.

Emanuel, K., R. Sundararajan, and J. Williams. 2008. "Hurricanes and global warming—Results from downscaling IPCC AR4 simulations." *Bull. Am. Meteorol. Soc.* 89 (3): 347–368. https://doi.org/10.1175/BAMS-89-3-347.

Enríquez, A. R., M. Marcos, A. Falqués, and D. Roelvink. 2019. "Assessing beach and dune erosion and vulnerability under sea level rise: A case study in the Mediterranean Sea." *Front. Mar. Sci.* 6: 4. https://doi.org/10.3389/fmars.2019.00004.

Feagin, R. A., D. J. Sherman, and W. E. Grant. 2005. "Coastal erosion, global sea-level rise, and the loss of sand dune plant habitats." *Front. Ecol. Environ.* 3 (7): 359–364. https://doi.org/10.1890/1540-9295(2005)003[0359:CEGSRA]2.0.CO;2.

Figlus, J., N. Kobayashi, C. Gralher, and V. Iranzo. 2011. "Wave overtopping and overwash of dunes." *J. Waterway, Port, Coastal, Ocean Eng.* 137 (1): 26–33. https://doi.org/10.1061/(ASCE)WW.1943-5460.0000060.

Fowler, H. J., S. Blenkinsop, and C. Tebaldi. 2007. "Linking climate change modelling to impacts studies: Recent advances in downscaling techniques for hydrological modelling." *Int. J. Climatol.* 27 (12): 1547–1578. https://doi.org/10.1002/joc.1556.

Frees, E. W., and E. A. Valdez. 1998. "Understanding relationships using copulas." *N. Am. Actuarial J.* 2 (1): 1–25. https://doi.org/10.1080/10920277.1998.10595667.

GEBCO (General Bathymetric Chart of the Oceans) Compilation Group. 2023. *GEBCO 2023 grid*. GEBCO Compilation Group. Liverpool, UK: British Oceanographic Data Centre (BODC).

Genest, C., and L.-P. Rivest. 1993. "Statistical inference procedures for bivariate Archimedean copulas." *J. Am. Stat. Assoc.* 88 (423): 1034–1043. https://doi.org/10.2307/2290796.

Graham, H., and D. Nunn. 1959. *Meteorological considerations pertinent to standard project hurricane, Atlantic and gulf coasts of the United States*. National Hurricane Research Project (Rep. No. 33). Washington, DC: United States Dept. of Commerce, United States Weather Bureau.

Gray, C. 2024. "Galveston sea levels rising faster than almost anywhere else, study finds." Accessed October 22, 2025. https://www.chron.com/gulf-coast/article/galveston-rising-sea-levels-venice-19441565.php.

Gringorten, I. I. 1963. "A plotting rule for extreme probability paper." *J. Geophys. Res.* 68 (3): 813–814. https://doi.org/10.1029/JZ068i003p00813.

Grotch, S. L., and M. C. Maccracken. 1991. "The use of general-circulation models to predict regional climatic-change." *J. Clim.* 4 (3): 286–303. https://doi.org/10.1175/1520-0442(1991)004<0286:TUOGCM>2.0.CO;2.

Hagemann, S., C. Chen, J. O. Haerter, J. Heinke, D. Gerten, and C. Piani. 2011. "Impact of a statistical bias correction on the projected hydrological changes obtained from three GCMs and two hydrology models." *J. Hydrometeorol.* 12 (4): 556–578. https://doi.org/10.1175/2011JHM1336.1.

Holland, G. J. 1980. "An analytic model of the wind and pressure profiles in hurricanes." *Mon. Weather Rev.* 108 (8): 1212–1218. https://doi.org/10.1175/1520-0493(1980)108<1212:AAMOTW>2.0.CO;2.

Holland, G. J., J. I. Belanger, and A. Fritz. 2010. "A revised model for radial profiles of hurricane winds." *Mon. Weather Rev.* 138 (12): 4393–4401. https://doi.org/10.1175/2010MWR3317.1.

Holthuijsen, L. H. 2007. *Waves in oceanic and coastal waters*. Cambridge, UK: Cambridge University Press.

IPCC (Intergovernmental Panel on Climate Change). 2023. *Climate change 2023: Synthetic report. contribution of working Groups I, II and III to the sixth assessment report of the intergovernmental panel on climate change*. Geneva: IPCC.

Jonkman, S. N., K. T. Lendering, E. C. van Berchum, A. Nillesen, L. F. Mooyaart, P. de Vries, M. van Ledden, A. Willems, and R. Nooij. 2015. "Coastal spine system—Interim design report."Accessed March 11, 2024. https://www.tamug.edu/ikedike/images_and_documents/20150620_Coastal_spine_ system-interim_design_report_v06.pdf.

Kalourazi, M. Y., S. M. Siadatmousavi, A. Yeganeh-Bakhtiary, and F. Jose. 2020. "Simulating tropical storms in the Gulf of Mexico using analytical models." *Oceanologia* 62 (2): 173–189. https://doi.org/10.1016/j.oceano.2019.11.001.

Ke, Q., et al. 2021. "An integrated framework of coastal flood modelling under the failures of sea dikes: A case study in Shanghai." *Nat. Hazard.* 109: 671–703. https://doi.org/10.1007/s11069-021-04853-z.

Kendall, M. G. 1938. "A new measure of rank correlation." *Biometrika* 30: 81–93. https://doi.org/10.2307/2332226.

Knutson, T. R., and R. E. Tuleya. 2004. "Impact of CO_2-induced warming on simulated hurricane intensity and precipitation: Sensitivity to the choice of climate model and convective parameterization." *J. Clim.* 17 (18): 3477–3495. https://doi.org/10.1175/1520-0442(2004)017<3477:IOCWOS>2.0.CO;2.

Kobayashi, N., M. Buck, A. Payo, and B. D. Johnson. 2009. "Berm and dune erosion during a storm." *J. Waterway, Port, Coastal, Ocean Eng.* 135 (1): 1–10. https://doi.org/10.1061/(ASCE)0733-950X(2009)135:1(1).

Krafft, D. R., B. C. McFall, J. A. Melby, and B. D. Johnson. 2025. "Lifecycle analyses of subaerial beach nourishments with concurrent nearshore placement of dredged sediment and the role of alongshore transport." *J. Waterway, Port, Coastal, Ocean Eng.* 151 (1): 1–10. https://doi.org/10.1061/JWPED5.WWENG-2152.

Kriebel, D. L., and R. G. Dean. 1993. "Convolution method for time-dependent beach-profile response." *J. Waterway, Port, Coastal, Ocean Eng.* 119 (2): 204–226. https://doi.org/10.1061/(ASCE)0733-950X(1993)119:2(204).

Larson, M., C. Donnelly, J. A. Jiménez, and H. Hanson. 2009. "Analytical model of beach erosion and overwash during storms." *Proc. Inst. Civ. Eng. Marit. Eng.* 162 (3): 115–125. https://doi.org/10.1680/maen.2009.162.3.115.

Larson, M., L. Erikson, and H. Hanson. 2004. "An analytical model to predict dune erosion due to wave impact." *Coastal Eng.* 51 (8–9): 675–696. https://doi.org/10.1016/j.coastaleng.2004.07.003.

Larson, M., J. Palalane, C. Fredriksson, and H. Hanson. 2016. "Simulating cross-shore material exchange at decadal scale. theory and model component validation." *Coastal Eng.* 116: 57–66. https://doi.org/10.1016/j.coastaleng.2016.05.009.

Lemos, G., M. Menendez, A. Semedo, P. Camus, M. Hemer, M. Dobrynin, and P. M. A. Miranda. 2020. "On the need of bias correction methods for wave climate projections." *Global Planet. Change* 186: 103109. https://doi.org/10.1016/j.gloplacha.2019.103109.

Li, F., P. H. A. J. M. van Gelder, J. K. Vrijling, D. P. Callaghan, R. B. Jongejan, and R. Ranasinghe. 2014. "Probabilistic estimation of coastal dune erosion and recession by statistical simulation of storm events." *Appl. Ocean Res.* 47: 53–62. https://doi.org/10.1016/j.apor.2014.01.002.

Lin, N., R. E. Kopp, B. P. Horton, and J. P. Donnelly. 2016. "Hurricane Sandy's flood frequency increasing from year 1800 to 2100." *Proc. Natl. Acad. Sci. U. S. A.* 113 (43): 12071–12075. https://doi.org/10.1073/pnas.1604386113.

Loarca, A. L., P. Berg, A. Baquerizo, and G. Besio. 2023. "On the role of wave climate temporal variability in bias correction of GCM-RCM wave simulations." *Clim. Dyn.* 61: 3541–3568. https://doi.org/10.1007/s00382-023-06756-0.

Lobeto, H., M. Menendez, and I. J. Losada. 2021. "Future behavior of wind wave extremes due to climate change." *Sci. Rep.* 11: 7869. https://doi.org/10.1038/s41598-021-86524-4.

Maraun, D. 2016. "Bias correcting climate change simulations—A critical review." *Curr. Clim. Change Rep.* 2: 211–220. https://doi.org/10.1007/s40641-016-0050-x.

Martzikos, N. T., P. E. Prinos, C. D. Memos, and V. K. Tsoukala. 2021. "Statistical analysis of Mediterranean coastal storms." *Oceanologia* 63 (1): 133–148. https://doi.org/10.1016/j.oceano.2020.11.001.

Melchiori, M. R. 2006. *Tools for sampling multivariate Archimedean copulas*. YieldCurve. Sante Fe, Argentina: Universidad Nacional del Litoral.

Merrell, W., et al. 2021. "Response to USACE Texas coastal study." Accessed July 17, 2024. https://idrt.tamug.edu/wp-content/uploads/2021/01/USACE-Response-Report-Ike-Dike.pdf.

Merrell, W., L. G. Reynolds, A. Cardenas, J. R. Gunn, and A. J. Hufton. 2011. "The Ike Dike: A coastal barrier protecting the Houston/Galveston region from hurricane storm surge." In *Macro-engineering seawater in unique environments: Arid lowlands and water bodies rehabilitation*, edited by V. Badescu and R. B. Cathcart, 691–716. Heidelberg, Germany: Springer.

Mull, J., and P. Ruggiero. 2014. "Estimating storm-induced dune erosion and overtopping along U.S. west coast beaches." *J. Coastal Res.* 298 (6): 1173–1187. https://doi.org/10.2112/JCOASTRES-D-13-00178.1.

NOAA (National Oceanic and Atmospheric Administration) and NCEI (National Centers for Environmental Information). 2023. *Coastal relief models (CRMs)*. Asheville, North Carolina: NOAA and NCEI.

Parkinson, R. W., and D. E. Ogurcak. 2018. "Beach nourishment is not a sustainable strategy to mitigate climate change." *Estuarine Coastal Shelf Sci.* 212: 203–209. https://doi.org/10.1016/j.ecss.2018.07.011.

Ranasinghe, R., D. Callaghan, and M. J. F. Stive. 2012. "Estimating coastal recession due to sea level rise: Beyond the Bruun rule." *Clim. Change* 110 (3–4): 561–574. https://doi.org/10.1007/s10584-011-0107-8.

Sallenger, A. H. 2000. "Storm impact scale for barrier islands." *J. Coastal Res.* 16 (3): 890–895.

Son, S., C. Xu, M. Davlasheridze, A. D. Ross, and J. D. Bricker. 2025. "Effectiveness of the Ike Dike in mitigating coastal flood risk under multiple climate and sea level rise projections." *Risk Anal.* 45: 2865–2894. https://doi.org/10.1111/risa.70060.

Sorensen, R. M. 2006. *Basic coastal engineering*. New York: Springer.

Sweet, W. V., et al. 2022. *Global and regional sea level rise scenarios for the United States: Updated mean projections and extreme water level probabilities along U.S. coastlines*. Silver Spring, MD: National Oceanic and Atmospheric Administration, National Ocean Service.

Teutschbein, C., and J. Seibert. 2012. "Bias correction of regional climate model simulations for hydrological climate-change impact studies: Review and evaluation of different methods." *J. Hydrol.* 456–457: 12–29. https://doi.org/10.1016/j.jhydrol.2012.05.052.

Um, M.-J., H. Kim, and J.-H. Heo. 2016. "Hybrid approach in statistical bias correction of projected precipitation for the frequency analysis of extreme events." *Adv. Water Resour.* 94: 278–290. https://doi.org/10.1016/j.advwatres.2016.05.021.

USACE Galveston District and GLO. 2021a. *Coastal Texas protection and restoration feasibility study—Final report*. Galveston, TX: USACE Galveston District.

USACE Galveston District and GLO. 2021b. *Coastal Texas protection and restoration feasibility study—Final report*. Appendix D—Engineering Design, Cost Estimates, and Cost Risk Analysis. Galveston, TX: USACE Galveston District.

USACE Galveston District and GLO. 2021c. *Coastal Texas protection and restoration feasibility study—Final report*. Appendix D—Annex 18: Beach and Dune Design and Drainage Report. Galveston, TX: USACE Galveston District.

van Rijn, L. C. 2009. "Prediction of dune erosion due to storms." *Coastal Eng.* 56 (4): 441–457. https://doi.org/10.1016/j.coastaleng.2008.10.006.

Wahl, T., N. G. Plant, and J. W. Long. 2016. "Probabilistic assessment of erosion and flooding risk in the northern Gulf of Mexico." *J. Geophys. Res.: Oceans* 121 (5): 3029–3043. https://doi.org/10.1002/2015JC011482.

Webster, P. J., G. J. Holland, J. A. Curry, and H. R. Chang. 2005. "Changes in tropical cyclone number, duration, and intensity in a warming environment." *Science* 309 (5742): 1844–1846. https://doi.org/10.1126/science.1116448.

Xie, L., S. Bao, L. J. Pietrafesa, K. Foley, and M. Fuentes. 2006. "A real-time hurricane surface wind forecasting model: Formulation and verification." *Mon. Weather Rev.* 134 (5): 1355–1370. https://doi.org/10.1175/MWR3126.1.

Zweers, N. C., V. K. Makin, J. W. de Vries, and G. Burgers. 2010. "A sea drag relation for hurricane wind speeds." *Geophys. Res. Lett.* 37 (21): L21811. https://doi.org/10.1029/2010GL045002.